### Title

Microtrabecular structure of the axoplasmic matrix: visualization of cross-linking structures and their distribution.




### Journal

The Journal of cell biology, 87(2 Pt 1)

### ISSN

0021-9525



### Authors

Ellisman, MH
Porter, KR



### Publication Date

1980-11-01

### DOI

10.1083/jcb.87.2.464

Peer reviewed

# Microtrabecular Structure of the Axoplasmic Matrix: Visualization of Cross-linking Structures and Their Distribution

MARK H. ELLISMAN and KEITH R. PORTER
*Department of Neurosciences, University of California, San Diego, School of Medicine, La Jolla, California 92093; and Department of Molecular, Cellular, and Developmental Biology, University of Colorado, Boulder, Colorado 80309*

ABSTRACT Axoplasmic transport is a dramatic example of cytoplasmic motility. Constituents of axoplasm migrate as far as 400 mm/d or at ~5 μm/s. Thin-section studies have identified the major morphological elements within the axoplasm as being microtubules, neurofilaments (100-Å filaments), an interconnected and elongated varicose component of smooth endoplasmic reticulum (SER), more dilated and vesicular organelles resembling portions of SER, multivesicular bodies, mitochondria, and, finally, a matrix of ground substance in which the tubules, filaments, and vesicles are suspended. In the ordinary thin-section image, the ground substance is comprised of wispy fragments which, in not being noticeably tied together, do not give the impression of representing more than a condensation of what might be a homogeneous solution of proteins. With the high-voltage microscope on thick (0.5-μm) sections, we have noticed, however, that the so-called wispy fragments are part of a three-dimensional lattice. We contend that this lattice is not an artifact of aldehyde fixation, and our contention is supported by its visability after rapid-freezing and freeze-substitution. This lattice or microtrabecular matrix of axoplasm was found to consist of an organized system of cross-bridges between microtubules, neurofilaments, cisternae of the SER, and the plasma membrane. We propose that formation and deformation of this system are involved in rapid axonal transport.

To facilitate electron microscope visualization of the trabecular connections between elements of axoplasm, the following three techniques were used: first, the addition of tannic acid to the primary fixative, $OsO_4$ postfixation, then en bloc staining in uranyl acetate for conventional thick or thin sections visualized in a high voltage electron microscope (HVEM) or in a conventional transmission electron microscope (TEM); second, embedding tissue in polyethylene glycol for thin sectioning, dissolving out the embedding medium from the sections and blocks, critical-point-drying (J. J. Wolosewick, 1980, *J. Cell Biol.*, 86:675–681.), and then observing the matrix-free sections with TEM or the blocks with a scanning electron microscope; and third, rapid freezing of fixed tissue followed by freeze-etching and rotary-shadowing with replicas observed by TEM. All of these procedures yielded images of cross-linking elements between neurofilaments and organelles of the axoplasm. These improvements in visualization should enable us to examine the distribution of trabecular links on motile axonal organelles.

Rapid translocations of formed elements occur within the long slender processes of nerve cells. The most rapid of movements within the cytoplasm of axons, the axoplasm, appears to involve the concomitant movement of protein, sulfated macromolecules, calcium, and vesicular organelles that resemble portions of the smooth endoplasmic reticulum (SER) (2, 12, 20, 23, 30, 42). The contention that "packages" of material are transported down the axon is supported by a large amount of data identifying different major macromolecular constituents that comprise five distinct rate classes of axonal transport (2, 27, 31, 55,



THE JOURNAL OF CELL BIOLOGY · VOLUME 87 NOVEMBER 1980 464-479

56). Insights gained through these biochemical analyses can be usefully combined both with observations on the rapid bidirectional movements of formed elements using high resolution light microscopy (8, 17, 18, 40), and with numerous electron microscope observations localizing specific components known to be rapidly transported to membrane-bounded organelles or inclusions (20). Therefore, information obtained about the process of neuroplasmic transport with different research techniques is consistent with a model of rapid axonal transport in which membranous compartments or containers (formed elements), associated protein, glycoprotein, mucopolysaccharide, and calcium move out of the perikaryon into a colinear array of neurofilaments and microtubules comprising the major and relatively static (slowest moving) components of the axoplasm (25, 42).

Morphological studies of the structure of axoplasm have revealed major elements common to the cytoplasm of other cell types in which rapid intracytoplasmic motility (streaming) is observed (3, 9, 10, 26, 45, 47, 49, 50, 59, 60). These common structural components include microtubules, intermediate filaments, mitochondria, membranous cisternae of various forms, and multivesicular bodies. Some investigators have noted "wispy" material emanating from microtubules and neurofilaments (35), especially after staining with ruthenium red (48) or lanthanum (4, 29).

Recent high voltage electron microscope (HVEM) examinations of cultured cells (41, 58) have revealed the larger and more easily identified organelles and inclusions to be suspended or contained in a trabecular lattice within the cytoplasmic ground substance. This finely divided component of the cytoplasm, when viewed stereoscopically in high voltage electron micrographs, appears to be composed of slender, interconnected strands from 40 to 100 Å in diameter and from 100 to 1,000-Å long, termed microtrabeculae. The interconnected microtrabeculae form a morphological network termed the microtrabecular lattice (MTL). These trabeculae appear to cyclically form, deform, and form again with the rapid and saltatory translocations of pigment granules in fish erythrophores (5, 33). This evidence, along with observations on the subtle but selective alterations in the form of the microtrabeculae in response to cold, cyclic cAMP, increased and decreased Ca, increased and decreased Mg, metabolic inhibitors, colchicine, cytochalasin, etc., is consistent with the concept of a dynamic structure (15, 33, 34).

Recognizing the potential importance of such a dynamic component interposed at the interface between either a rapidly moving pigment granule or axoplasmic cisternae on the one hand and the relatively static microtubules or neurofilaments on the other, we undertook studies aimed at examining the three-dimensional structure of the MTL in axoplasm. In the studies reported here, we have examined the fine structural details of interlinking structures between neurofilaments, microtubules, various types of axonal cisternae, and the plasma membrane. Little is seen of interlinking structures in conventionally prepared thin sections of cells from tissues because the electron scattering of the epoxy resin coincides with that of the elements of this lattice. To better visualize the distribution of this fine lattice in axoplasm, it was necessary to adapt several new electron microscope techniques.

The first experiments detailed the morphology observed after the use of staining procedures designed to enhance the electron density associated with the axonal microtrabecular elements as visualized in thick epoxy sections with the aid of HVEM. Epoxy sections of axons were also examined after rapid-freezing and freeze-substitution to demonstrate that the axonal lattice is not an aldehyde fixation artifact. Second, we used a water-soluble embedding technique adapted to enable the examination of the ultrastructure of thin and thick tissue sections by standard transmission electron microscopy (TEM) and HVEM (57). Materials embedded in such soluble matrices were examined with high resolution scanning electron microscopy (SEM). Third, we used a cryofracture rotary-shadow replication technique for visualization of the same elements after rapid-freezing (24). From the combined information obtained through these approaches, we have constructed a model of the cytoskeleton in axoplasm.

## MATERIALS AND METHODS

### Fixation of Tissues

ALDEHYDE-FIXED TISSUE: All tissues used in these experiments were from Sprague-Dawley rats, 75–200 g, anesthetized with either Nembutal (50 mg/kg intraperitoneally [i.p.]) or chloralhydrate (10 mg/100 g i.p.), and perfused through the left ventricle with an oxygenated Ringer's solution entering the animal at 37°C (13) and flowing until atrial outflow was clear (45 s to 1 min). The Ringer's rinse was immediately followed by the primary fixative solution, which consisted of 2% glutaraldehyde, 1% paraformaldehyde in 0.15 M sodium cacodylate, pH 7.3. In some experiments, this fixative was supplemented with 4% tannic acid (low molecular weight ~314, $[C_{14}H_{10}O_9]$ obtained from Mallinckrodt Inc., St. Louis, Mo.). All perfusates were freshly prepared, warmed to 37°C, briefly oxygenated by bubbling with 95% air–5% $CO_2$, and then perfused through the animal for 3–5 min. Immediately after the perfusion, dorsal and ventral spinal roots and spinal cord were carefully removed by dorsal laminectomy and placed in the same fixative solution at 4°C to total 1 h of fixation. During this hour in fixative, 2- to 5-mm-long segments were carefully cut from spinal roots. The tissue was then washed in 0.15 M sodium cacodylate buffer for 5 min four times and placed in 1% $OsO_4$ in the same buffer for 1 h at 4°C.

RAPIDLY FROZEN FREEZE-SUBSTITUTED TISSUE: After anesthetization of rats, a dorsal laminectomy was performed to expose the spinal cord and dorsal roots. Cross-sectioned segments of the cord were quickly removed and then frozen against the silver cold finger of a quick-freezing apparatus similar to that described by Van Harreveld and coworkers (53). The tissue was substituted for 36 h at −80°C in acetone containing 2% $OsO_4$ (Sigma Chemical Co., St. Louis, Mo.), warmed slowly over a 3-h period to room temperature, washed with fresh acetone, and embedded in Epon-Araldite resin.

### Techniques for Visualization of Microtrabecular Elements

#### En Bloc Staining

After a wash of 5 min in buffer and then two washes of 5 min in double-distilled $H_2O$, the tissues were stained en bloc with one of the following procedures: (*a*) 0.5% aq uranyl acetate (UA) for 1 h at room temperature, (*b*) 1% aq: ferric chloride ($FeCl_3$) for 20 min at room temp.; or (*c*) 0.5% aq: tannic acid (low molecular weight) for 30 min at room temperature. The tissues were then washed briefly in double-distilled $H_2O$ and dehydrated in either an ethanol or acetone series (20, 50, 70, 90, 100%) for 10 min at each step and subsequently infiltrated and embedded with either Spurr or Epon-Araldite resin.

SECTIONING AND GRID STAINING OF EPOXY-EMBEDDED MATERIAL: The tissues were mounted on acrylate blocks. Ultra thin sections from 300- to 800-Å thick were cut on an American Optical Ultracut microtome (American Optical Corp., Southbridge, Mass.) and mounted on bare 200- or 300-mesh copper grids. Sections were then either viewed directly or first counter-stained with 2% UA (aq) for 20 min at 45°C followed by lead citrate for 5 min. Alternatively, some sections were stained with 0.5% UA (in 70% methanol) at 60°C for 30 min.

#### Polyethylene Glycol Embedding

Spinal roots in double-distilled $H_2O$ fixed as detailed above were placed in a mixture of four parts polyethylene glycol (PEG) (4,000 mol wt), one part PEG (6,000 mol wt) and five parts $H_2O$ held at 37°C with agitation. After 30 min, the roots were infiltrated with a mixture of four parts PEG 4,000 and one part PEG

6,000 at 60°C for 1 h followed by fixation in a fresh mixture of the same makeup for an additional 30 min. The tissue was then transferred to an aluminum weighing pan filled with the fresh PEG mixture and cooled quickly to 15–20°C in a freezer. The ideal concentration of PEG and the necessary infiltration time was determined experimentally.

SECTIONING, CRITICAL-POINT-DRYING, AND CARBON STABILIZATION OF EMBEDDED TISSUES: Once the PEG had solidified, the tissue was mounted on an acrylate block with an alpha-cyanoacrylate adhesive (Super Glue, Woodhill Chemical Sales Corp., Cleveland, Ohio) and rough trimmed with a razor blade. The final blocks were precision trimmed in the ultramicrotome so that the block face was composed of 100% tissue (~1 × 3 mm). The block was then thin sectioned on an American Optical Ultracut (American Optical Corp.) at 30 mm/s with glass knives having knife angles of 35° and a clearance angle of 9°. Care must be taken because the block face is extremely hygroscopic and any contact with moisture instantly dissolves it. Triton X-100 (0.05–0.4%) in double-distilled $H_2O$ may be added to the boat trough to reduce surface tension, thus allowing the sections to be cut "underwater." The Triton may be avoided, however, if sections are submersed immediately after cutting with an eyelash manipulator (all images presented in this paper were obtained without Triton). Sections from 400 to 2,000-Å thick can be cut and, though the exact thickness cannot be judged by interference colors, it can be closely estimated by observing the section's characteristics in the boat.

The sections are transferred from the bottom of the trough (where they are visualized with a back lighting system) to a petri dish full of double-distilled $H_2O$ via a Pasteur pipette (sections must be kept underwater at all times) and then manipulated with eyelash manipulators and a × 10 stereoscope onto either a poly-L-lysine (0.1% aqueous)-treated Formar-coated (0.1%) copper grid or a polybutene (1% in xylene)-coated folding grid (Pelco, Ted Pella Inc., Tustin, Calif.). The secured sections were then placed in a grid holder and transferred to fresh double-distilled $H_2O$. The temperature was slowly raised to 50–60°C for 5 min, and then the sections were dehydrated in a graded series of ethanol (20, 50, 70, 90, 100%) and critical-point-dired with $CO_2$ in a Balzer-Union CPD apparatus (Balzers Corp., Nashua, N. H.). The dired sections were then rotary-coated on both sides with 100 Å of carbon in a Balzers 350 vacuum evaporator. Care was taken to shield the samples from thermal damage during carbon coating. The samples were viewed at 80 and 100 keV on a JEOL 100CX with an $LN_2$ cold trap and an $LN_2$ anticontamination device at a beam current from 30 to 140 μÅ and at 1,000 keV with the HVEM located in Boulder, Co. Because the absence of an embedding matrix greatly reduces background electron scattering and, thus, greatly increases contrast, most routine microscopy was performed with a 100 or 200 μm objective aperture.

PREPARATION FOR SEM: Tissues fixed and embedded in PEG were mounted on blocks, trimmed to include tissue only, and then sectioned to the desired depth, as determined by collected sections viewed in a light microscope. The final sections taken from the block were cut only 400 Å at a time to produce a mirror-smooth block face. The tissue was then removed from the microtome, separated from the block, and placed in double-distilled $H_2O$. The temperature of the water was then slowly raised to 40°C over a period of 15 min. The tissue was washed for 4 min three times with double-distilled $H_2O$ at 40°C, and subsequently dehydrated in a 40°C ethanol series (20, 50, 70, 80, 90, 100%), replaced slowly with acetone, and critical-point-dried in $CO_2$ with a Balzers-Union CPD apparatus. Tissues thus dried were mounted on aluminum stubs and coated with 20–50 Å of Au-Pd followed by 50–100 Å of carbon with a Balzers vacuum evaporator. The samples were examined on a JEOL 100 CX equipped with a high-resolution automatic scanning imaging device (ASID) at up to × 200,000 at an accelerating voltage of 60 keV and beam current of 1–40 μÅ.

## Freeze-Fracture Deep-Etching

Spinal roots were aldehyde fixed as described above and cut into 1–2-mm segments, and then individually frozen on solid-gold specimen supports (Balzers Corp.) by rapidly pressing them against a copper block cooled by a nitrogen slush (52, 53) or liquid helium (24). The frozen specimens were freeze-fractured in a Balzers 300 freeze-etching device equipped with a turbomolecular pump, electron guns, a quartz-crystal thin-film monitor, a rotating specimen stage, and a time- and heat-limiting electronic shutter (16). The cleavage was propagated at an angle slightly oblique to the longitudinal axis of the nerve fiber to expose cross-fractured expanses of axoplasm and to enable location of the optimally frozen surface that had contacted the supercooled block. During the fracturing, the specimen stage temperature was −105°C, whereas during the etching, the temperature was raised to −95°C for a period of 1–3min followed by the rotary-shadowing, which was terminated after the quartz-crystal monitor reached a value of 220 Hz. Replicas were floated on $H_2O$ and cleaned with bleach (Clorox), and with 40% chromic acid. Micrographs from these preparations are presented here as photographic reversals.

## RESULTS

Difficulties are immediately encountered when one is looking in nerve cells for a morphological equivalent of the microtrabecular system described in cultured cells, using conventional thin sections cut from epoxy-embedded tissues. Little of the lattice work is seen because the electron scattering of the epoxy resin coincides with that of the elements of the lattice. To increase the electron scattering of the trabecular elements in epoxy sections, we have adapted various en bloc staining procedures, wherein tissues are incubated with a heavy metal, such as uranyl acetate, before infiltration with plastic. When thin sections of material prepared in this manner are examined, more of the lattice is visible (Figs. 1 and 2). In cross sections of nerve axons (Fig. 1), it is easy to observe mitochondria embedded in microtubule-rich zones and numerous 100-Å neurofilaments. These better-known components appear to be embedded in a matrix of wispy material which, in not being noticeably tied together, might be interpreted as a condensation of an otherwise homogeneous solution of protein. In a longitudinal section (Fig. 2), such microtubules, neurofilaments, cisternae of the SER, multivesicular bodies, and other organelles and inclusions are identified. Here, too, a periodic cross-bridging component is visible in the spaces between these elements. This is similar to one delineated by lanthanum staining of crayfish axons (4). Using such en bloc stained material in conjunction with stereo HVEM, we examined the three-dimensional distribution of these wispy elements within sections of the cytoplasm of neurons.

## Stereo HVEM of Axoplasm

The three-dimensional form of axons and their contents may be visualized in one set of stereo pairs (Fig. 3). In such images, various forms of SER and the continuity of neurofilaments and microbubules may be appreciated. Such stereo pairs allow one to compare the relative dimensions of the cisternae of the SER and multivesicular bodies with the spaces between the longitudinally deposed neurofilaments and microtubules. When a 0.5-μm-thick longitudinal section through an axon is observed, the richness of interconnecting elements between neurofilaments may be appreciated (Fig. 4). These interconnecting wispy strands of trabeculae appear to radiate into the ground substance at right angles to the microtubules and neurofilaments with a periodicity of ~425 Å (Fig. 4). The periodic cross-bridging component is continuous with similarly staining material coating the microtubules and neurofilaments. Multivesicular bodies are also suspended in the meshwork of filamentous components (Fig. 5). At higher powers, the trabecular connections to plasma membrane and cisternae of the SER are visualized (Fig. 6). Specialized connections to the plasma membrane are seen in the region of the node of Ranvier (Figs. 3 and 7). Here, with appropriate staining and HVEM visualization, one finds that the so-called subaxolemmal density (38) is composed of circumferentially deposed 40–50-Å filaments forming a fibrous belt just beneath the plasma membrane (11) and connected to the axolemmal matrix deeper in the axoplasm. Elements of the SER, embedded in and coated by this matrix, are found in a variety of forms, ranging from individual vesicles to very elongated varicose cisternae with numerous cross-bridging connections (Figs. 6 and 7). It appears that even the smallest vesicular cisternae of SER are large in diameter when compared with the average distance between adjacent

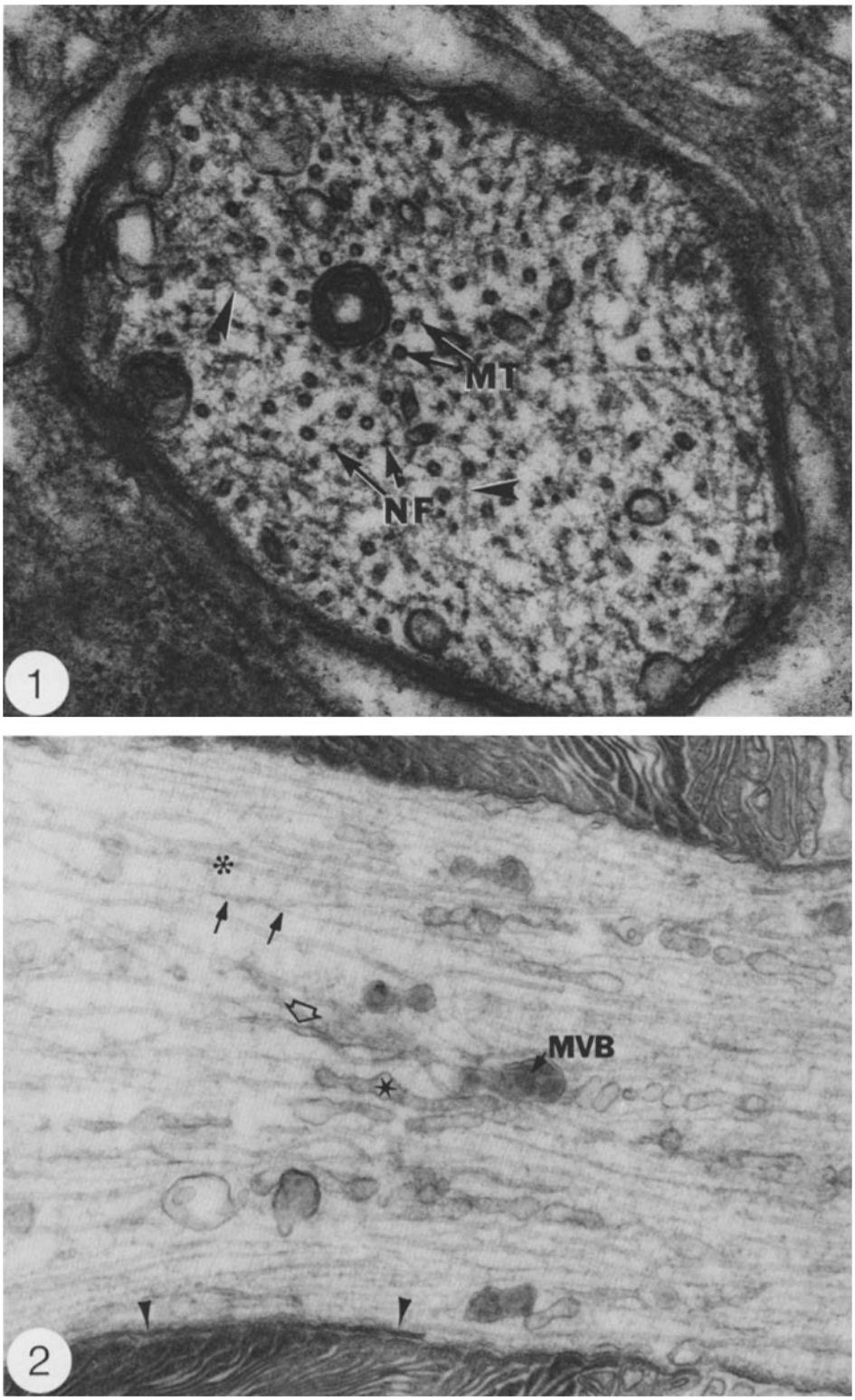


FIGURE 1 Conventional thin cross section of an axon from peripheral nerve. In such sections, it is easy to observe mitochondria embedded in microtubule-rich zones (*MT*), numerous 100-Å neurofilaments (*NF*), and wispy fragments of the cytoplasmic ground substance (arrow heads). × 80,000.

FIGURE 2 Conventional longitudinal thin section from a myelinated axon near a node of Ranvier. Microtubules (asterisk), neurofilaments (arrows), elongated varicose cisternae resembling a portion of the SER (star), and multivesicular bodies (*MVB*) are identified. An elongated subaxolemmal SER cisterna is visible adjacent to the paranodal junction (arrowheads). Note the periodic wispy cross-bridging components visible in the spaces between the other axoplasmic components. × 50,000.

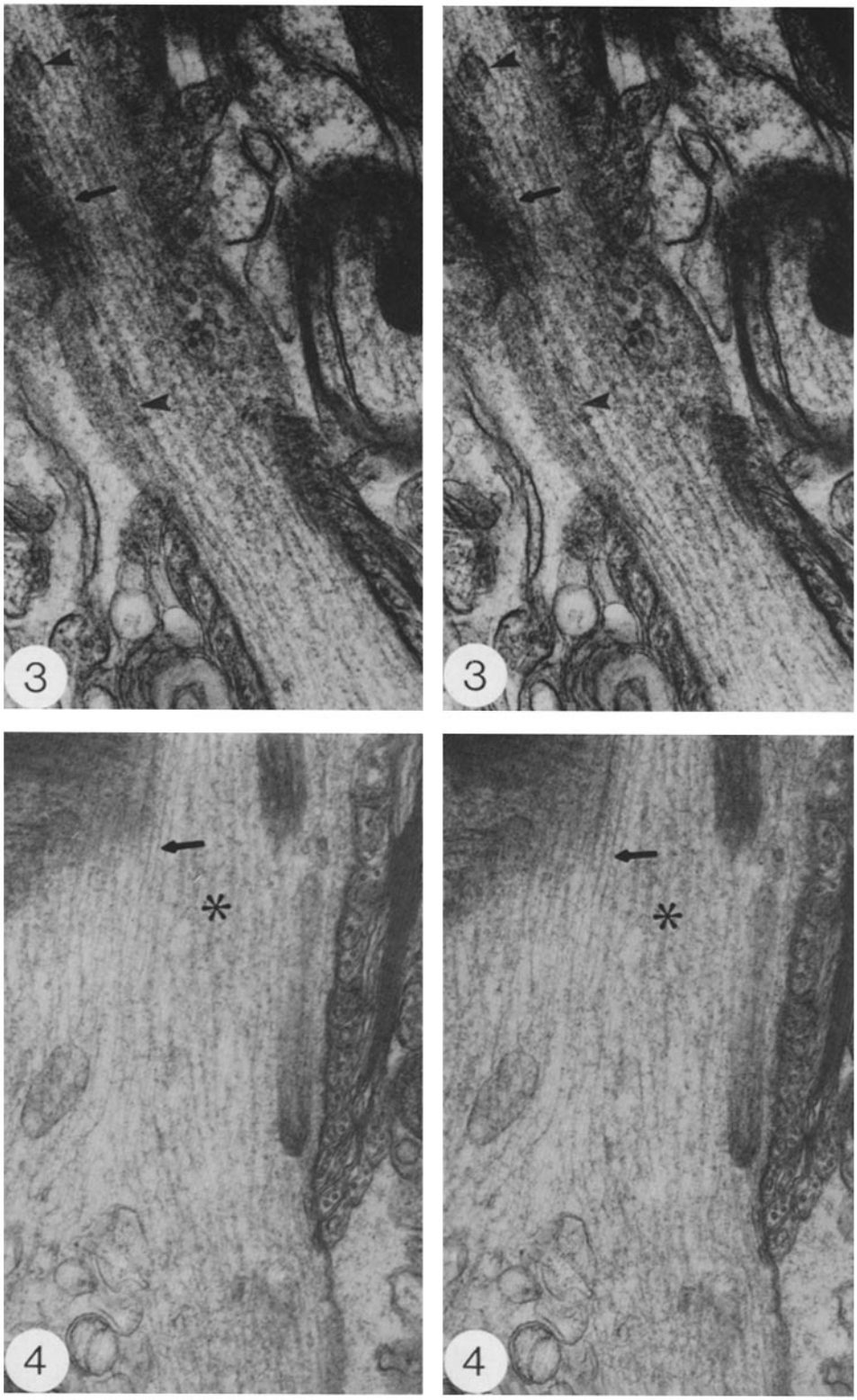


FIGURE 3 HVEM stereo pair micrographs of a 0.75-μm-thick section capturing nearly an entire node of Ranvier in a longitudinal section. Stereo viewing with a two-lens stereo viewer is recommended. When such images are fused, the continuity of neurofilaments (arrow) may be appreciated. Note the dimensions of the SER cisternae (arrowheads) and the multivesicular body relative to spacing between microtubules. × 35,000.

FIGURE 4 HVEM stereo pair micrographs of a longitudinal thick section through an axon in the central nervous system, near a node of Ranvier. When viewed stereoscopically, periodic cross-bridges between neurofilaments (arrow) and microtubules (asterisk) are visible. × 40,000.

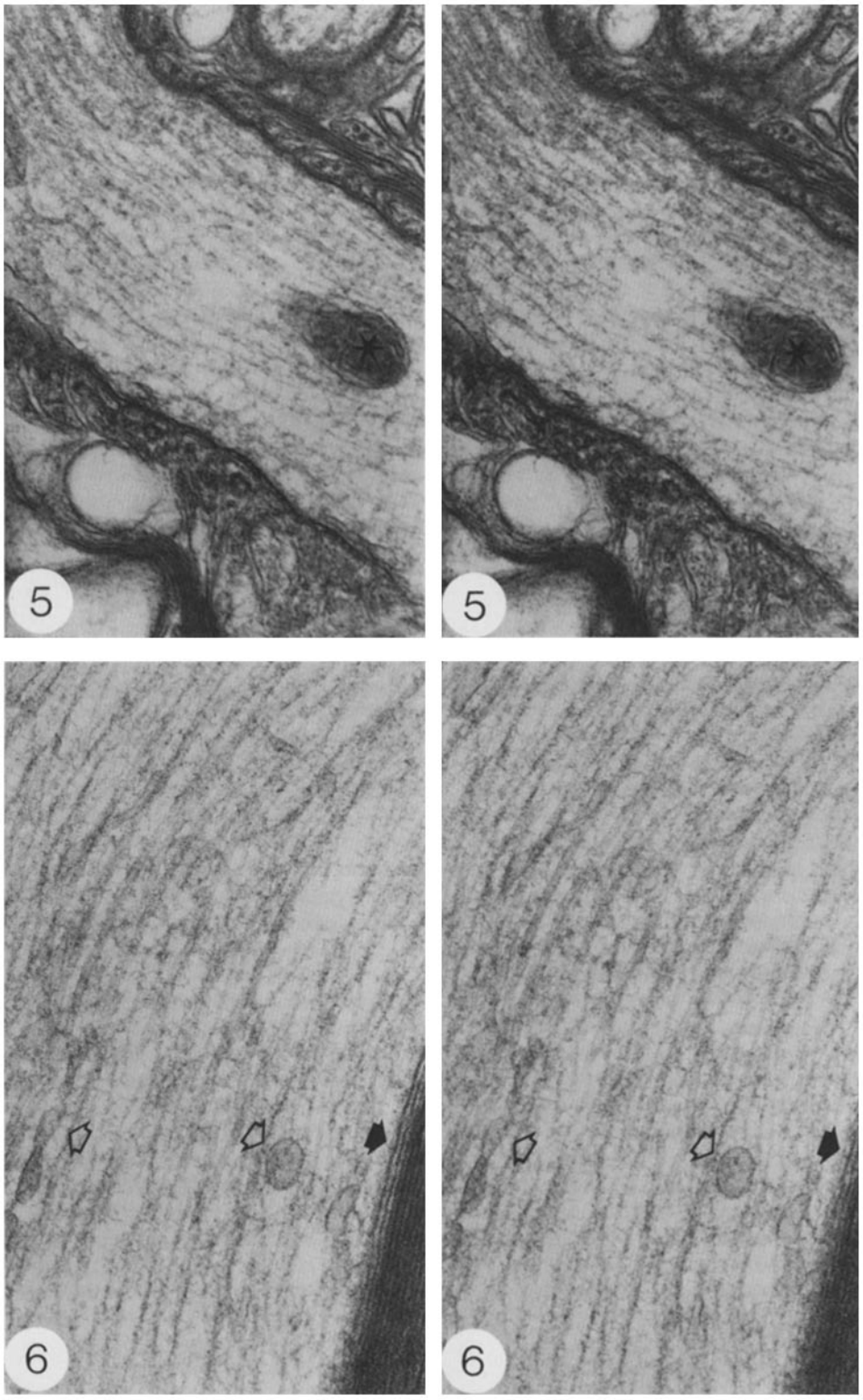


FIGURE 5 HVEM stereo pair micrographs illustrating a multivesicular body (star) embedded in the axoplasmic matrix near a node of Ranvier from a rat spinal cord ventral horn. × 50,000.

FIGURE 6 HVEM stereo pair micrographs of longitudinal thick section through a myelinated peripheral nerve axon. Linkages to the plasma membrane (solid arrows) and cisternae of axonal SER (open arrows) are visible. × 75,000.

interconnected filaments (Fig. 8). Often, the mesh appears disconnected on only one end of such compartments. In fact, images of such vesicles give one the impression that the trabecular connections may be "unzipped" or disconnected, enabling vesicles to pass down the axonal column. These linkages between microtubules or neurofilaments and cisternae are asymmetrically distributed not only on many small vesicles, but also on elongated varicose cisternae (Fig. 6) and multivesicular bodies (Fig. 5), often with a clearly identifiable loose end and an identifiable cross-linked end.

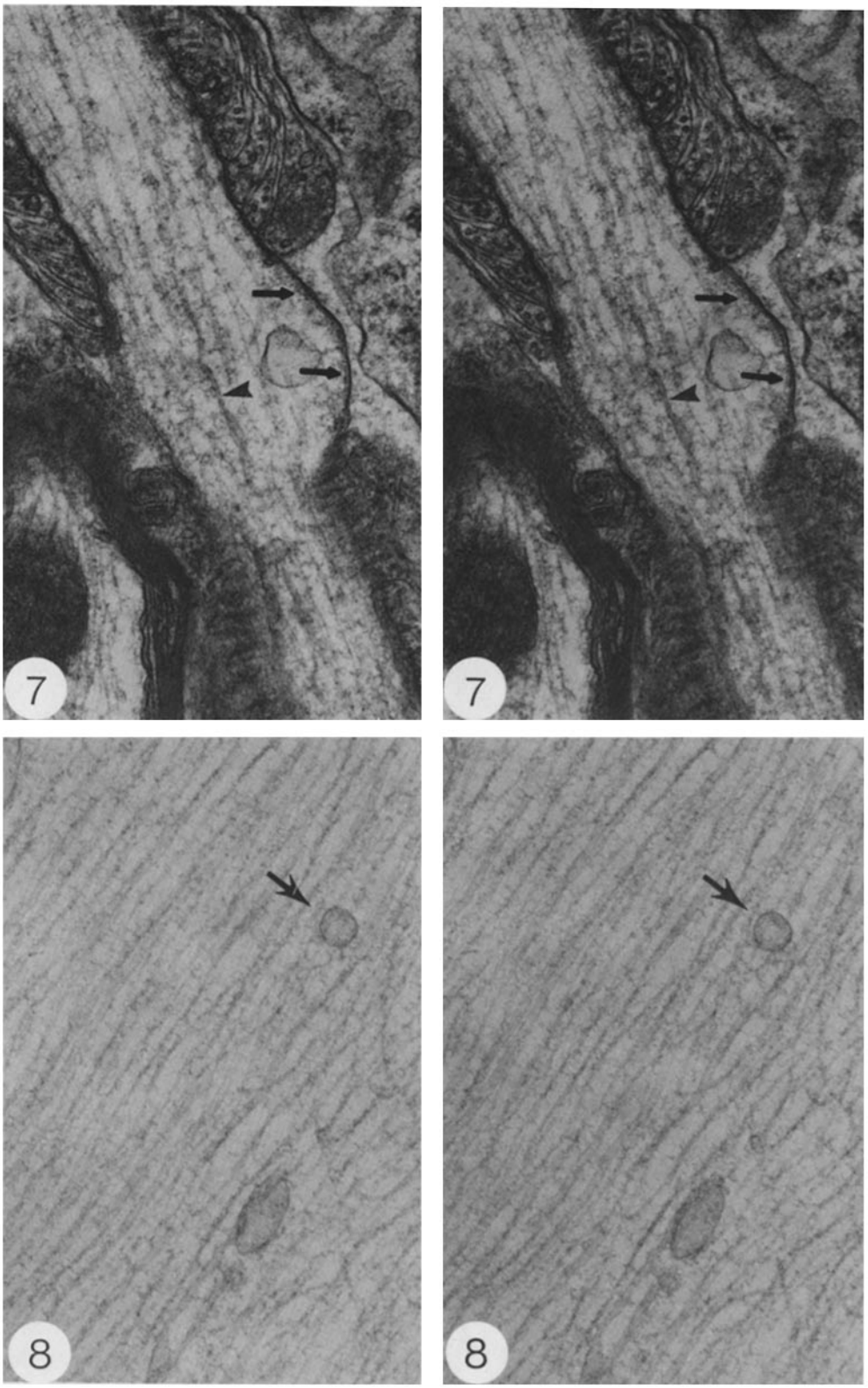


FIGURE 7 HVEM stereo pair micrographs of a central nervous system node of Ranvier. Note that the specialization of the axolemma at the nodal membrane is composed of a band of fine filaments seen here in cross section (arrows). Also visible in this micrograph is an example of the varicose or stringy form of axonal SER cisternae (arrowheads). × 45,000.

FIGURE 8 High magnification HVEM stereo pair micrographs of peripheral nerve axoplasm. Many small vesicular fragments of the SER (arrow) are larger in diameter than the average distance between adjacent neurofilaments and microtubules. The cross-bridging connections are often disconnected on one end of such cisternae. × 70,000.

## Morphology of the Axoplasmic Matrix after Fixation by Freezing

An earlier report on the form of the MTL in cultured cells after various fixation procedures included the demonstration of its preservation after fixation by freezing (58). Because in this study we are dealing with a tissue system in which axoplasm is highly differentiated for translocation of materials, we have included observations on rapidly frozen freeze-substituted material. Images of sections of axoplasm from tissue thus prepared (Fig. 9) are not significantly different from those of conventionally prepared glutaraldehyde-fixed material. Although it appears to be more difficult to impart electron contrast to the fine cross-bridging material between axonal elements, their presence is easily confirmed. These observations support our contention that, in this tissue system, as in the cultured cell, the MTL is not an artifact of an aldehyde-induced condensation of protein.

## The Microtrabecular Matrix of Axoplasm After Tannic Acid Mordanting

The stereo images detailing the distribution of cross-bridging trabeculae in the en bloc-stained material discussed above have increased our understanding of the three-dimensional relationship between axonal components. Our previous experiences examining similar fine details in cultured cells, however, suggest that the entire extent of the lattice was either not preserved or not visualized in these preparations. Therefore, we used a glutaraldehyde–tannic acid primary fixation (43, 44), both to increase the amount of electron-dense material adhering to axoplasmic components as a result of subsequent en bloc staining (tannic acid mordanting) and to better preserve actin (39). The stereo images of peripheral nerve prepared in this manner demonstrate that the electron contrast of matrix elements within axoplasm is clearly enhanced, especially when compared with myelin, which is normally stained much darker than axoplasm (cf., Fig. 10 and Fig. 7). At high magnification, the increased visibility of cross-bridging slender trabeculae and lattice material coating microtubules, neurofilaments, and cisternae may be appreciated (Fig. 11). There are more cross-bridges visible and/or preserved in these glutaraldehyde–tannic acid–fixed preparations. However, even with this procedure, designed to enhance contrast and improve preservation, one is unsure about how much material is left that has electron-scattering properties similar to those of the embedding matrix and is, therefore, still not visible.

## Visualization of the Axoplasmic Matrix in Preparations from which the Embedding Matrix is Removed

Not satisfied with just increasing the electron density of axonal components, we adapted a method designed to allow the observation of sections without the inherent noise of an embedding matrix. This involved embedding in PEG as detailed above. PEG is a water-soluble embedding material from which thick or thin sections may be cut and the embedding matrix subsequently dissolved away. After dehydration, the sections may be critical point dried and then stabilized with a layer of carbon on each side. Although it is technically more difficult to cut and process sections from this material, good preservation of ultrastructure is maintained. For example, at low magnifications, some of the common cellular constituents of peripheral nerve may be recognized and the quality of their

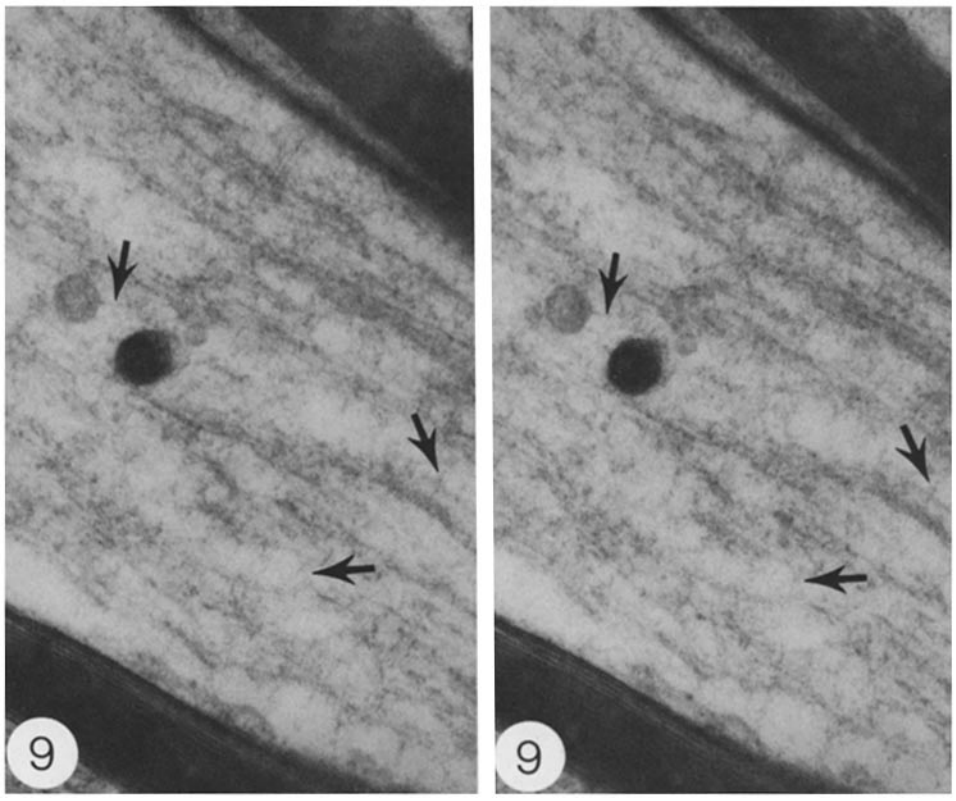


FIGURE 9 Longitudinally sectioned myelinated axon from rapidly frozen, freeze-substituted rat spinal cord. The arrows point out trabecular cross-linking elements within the axoplasm. × 25,000.

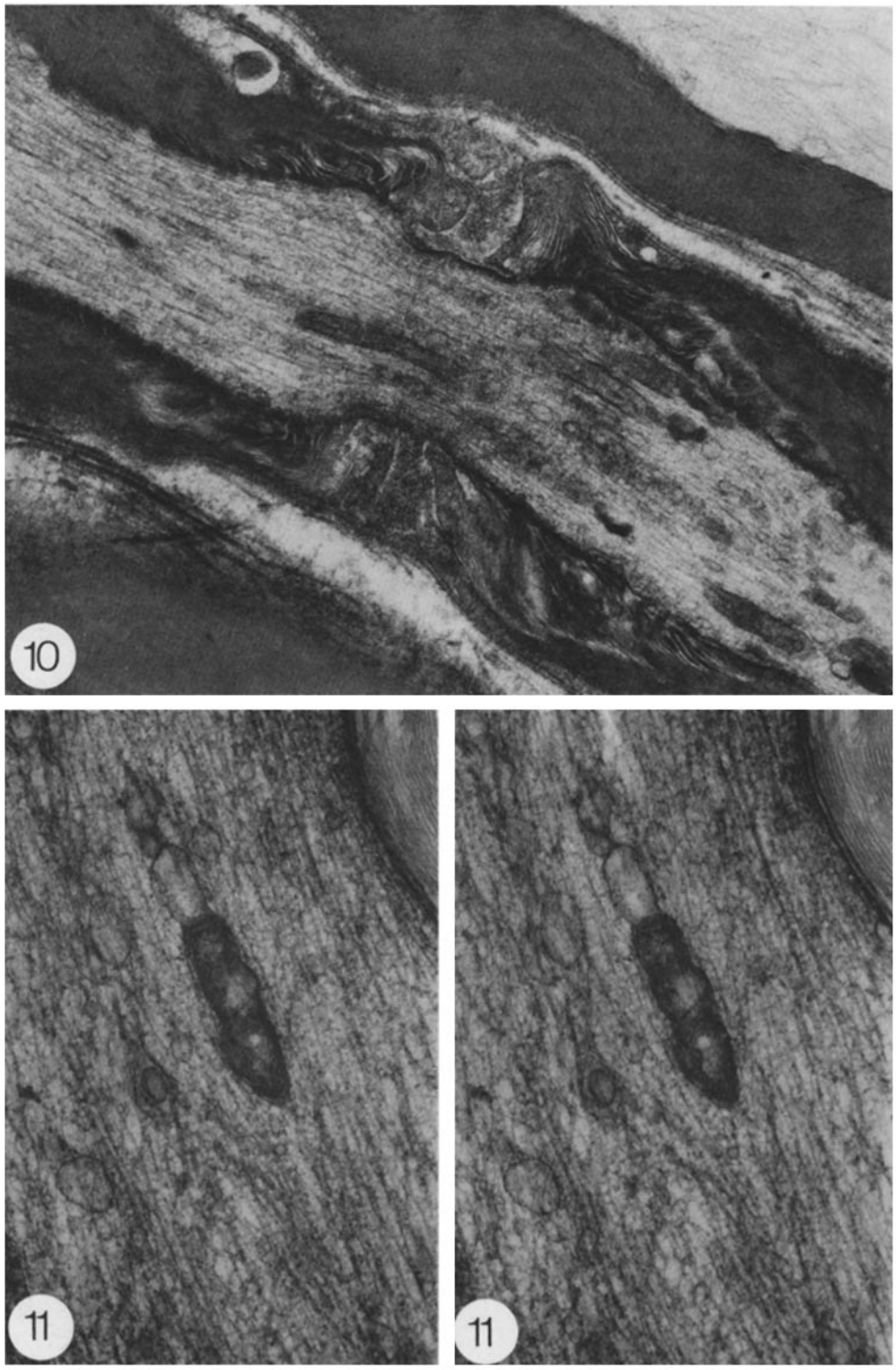


FIGURE 10 Low magnification of peripheral nerve in the vicinity of a node of Ranvier after glutaraldehyde-tannic acid fixation. Note that the electron density of the axoplasm is greatly enhanced over conventional preparations when compared with adjacent myelin. × 20,000.

FIGURE 11 High magnification of axoplasm fixed with glutaraldehyde-tannic acid and then en bloc stained with uranyl acetate. Note the extensive cross-bridging between axoplasmic components. × 45,000.

preservation assessed (Fig. 12). This micrograph includes a node of Ranvier, Schwann cell cytoplasm, microvilli of the Schwann cell over the node, and vesicular organelles most notable in the adjacent unmyelinated fibers. Remarkably, the loss of differential contrast between microtrabecular elements and the embedding matrix is overcome in these specimens from which the embedding matrix has been washed out. At higher magnification (Fig. 13), it is apparent that the number of trabecular cross-bridges between tubules and neurofilaments is much greater than that seen in epoxy-embedded sections. These


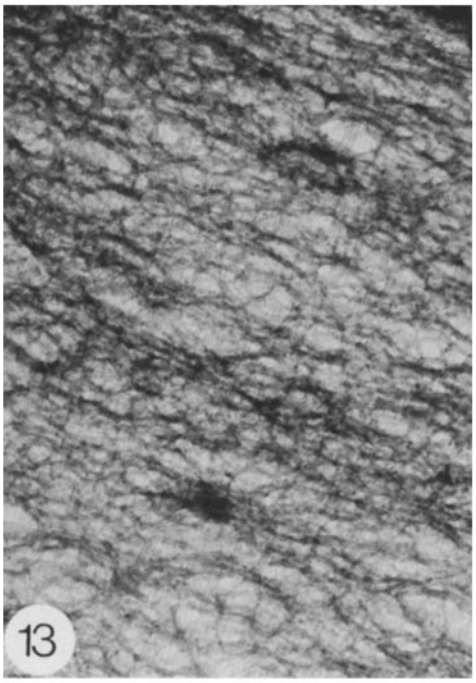


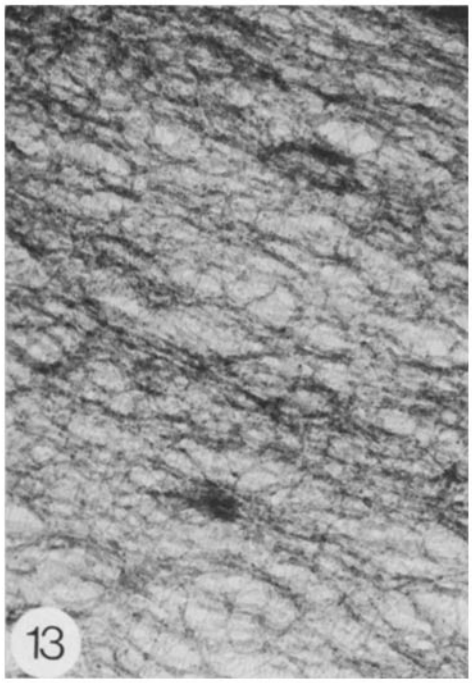


FIGURE 12 Low magnification of a section cut from PEG-embedded peripheral nerve demonstrating integrity of tissue in the vicinity of a node of Ranvier. Note the microvilli (*MV*) over the nodal membrane, the Schwann cell cytoplasm (*SC*), and the unmyelinated fibers (*UM*). × 17,000.

FIGURE 13 Higher magnifications of PEG section illustrating trabecular cross-bridging similar to that found in cultured cells viewed without an embedding matrix. × 50,000.

slender strands have an appearance not unlike the strands of trabeculae observed in non-PEG, whole mounted critical point dried, cultured cells (58). In these preparations, as in the cultured cell, the lattice material appears as a coating on the better-known components. Connections to large vesicles or cisternae are also visible in these preparations (Fig. 14).

Similar preparations derived from PEG-embedded tissue may be examined in the SEM after removal of the embedding matrix. For these purposes, we have found it most useful to cut a large block face, and then save, not the sections, but the block face, removing the polyethylene glycol (see Materials and Methods) and further process for SEM, as detailed above. Where axons have been sectioned open, the fibrous nature of the axoplasm may be readily appreciated (Figs. 15 and 16). At higher magnifications, neurofilaments and microtubules may be recognized, as well as fine lateral projections corresponding to the trabecular elements discovered by the other techniques described above. The preparation of PEG-embedded blocks of tissue for SEM is far easier and faster than preparing sections of PEG-embedded material for the TEM. The resolution, however, is limited by factors inherent in all scanning microscopes contributing to secondary electron emission characteristics (19), as well as by the resolution of the SEM, and is, therefore, not quite as good as in the sectioned material.

### *Freeze-Etched and Rotary-Shadowed Preparations of Axoplasm*

The third technique that we have used to visualize the microtrabecular matrix of axoplasm is the formation of replicas by freeze-etching and rotary-shadowing (Figs. 17 and 18). If preparations are aldehyde-stabilized and then rapidly frozen against a copper block in slush point nitrogen (52, 53) or at liquid helium temperatures (24), rather little deformation resulting from ice crystal formation is notable. In such preparations of axoplasm, numerous cross-bridges connecting microtubules, mitochondria, and neurofilaments may be recognized. Also notable in these preparations is the specialization of the cell cortex or region between the axolemma and axoplasm. This region of transition between the cell membrane and the cytoskeleton-cytomusculature appears to contain a high concentration of nonetchable material ~150-Å thick into which the cross-bridging components of axoplasm are inserted.

In summary, the most important new information resulting from our examination of the axoplasmic matrix is the following: (*a*) In axoplasm, the cytoplasmic ground substance takes the form of a system of trabecular cross-linkages between the larger formed elements. (*b*) Cross-linkages have been visualized by a variety of electron microscope techniques and exhibit very similar forms. These cross-bridges, however, are more difficult to see in conventionally prepared, epoxy-embedded material. (*c*) These trabecular cross-linkages are preserved after fixation by both aldehydes and freezing. (*d*) The distribution of the trabecular cross-linkages visualized in axoplasm appears to be highly periodic along both neurofilaments and microtubules. (*e*) The system of lateral projections from tubules and filaments creates a relatively uniform axonal matrix by providing for regularity in spacing between the neurofilaments and tubules. (*f*) This system of trabecular cross-linkages is continuous with the previously described "wispy fragments" that emanate from and coat the surface of the major formed elements within

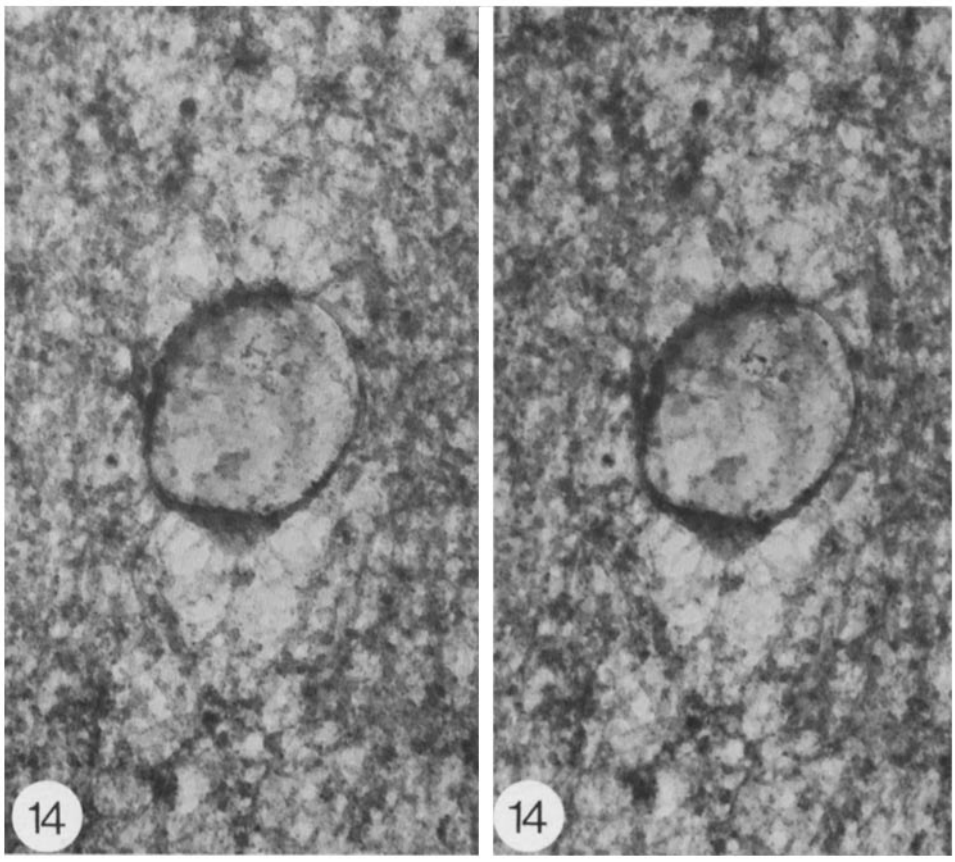


FIGURE 14 Stereo pair micrographs of PEG section illustrating connections of the cross-bridging lattice to a membrane bound cisterna. × 50,000.

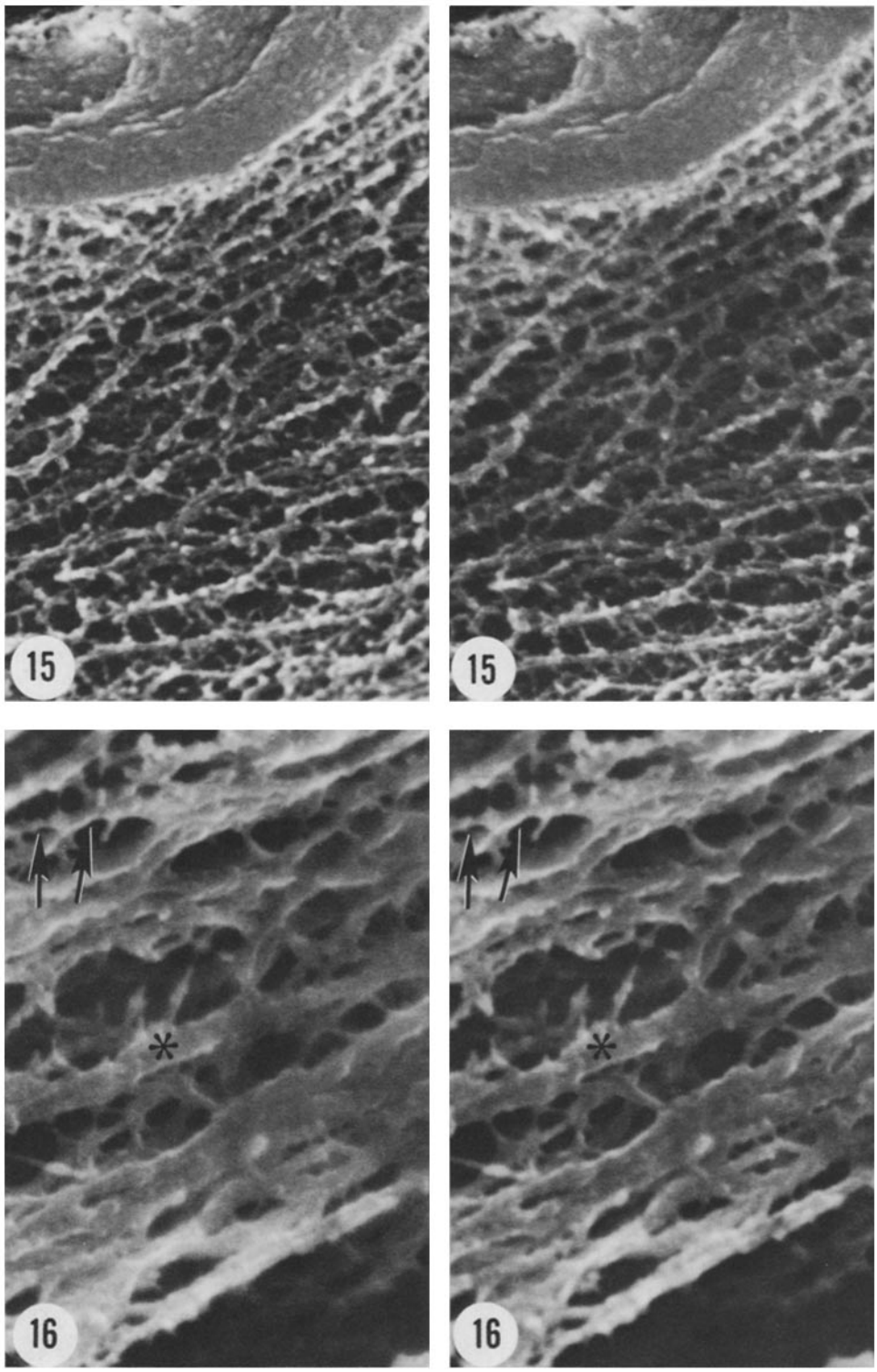


FIGURE 15 Stereo pair of scanning electron micrographs of the block face from which PEG sections have been cut. Note the numerous lateral connections between neurofilaments and microtubules. × 60,000.

FIGURE 16 Higher magnification scanning electron micrograph of axoplasm from a PEG preparation demonstrating numerous lateral projections from microtubules (asterisk) and neurofilaments (arrows). × 200,000.

axoplasm. (*g*) Many fragments of axonal SER (presumed transport compartments) visualized within axoplasm are larger in diameter than the spaces between the trabecularly connected fascicles of microtubules or neurofilaments. (*h*) The trabecular linkages seen between microtubules or neurofilaments and various forms of SER cisternae or multivesicular bodies are asymmetrically distributed, often with clearly identifiable connected and loose ends.

These points are summarized in Fig. 19, a three-dimensional model of the axoplasmic matrix (see figure legend for details.)

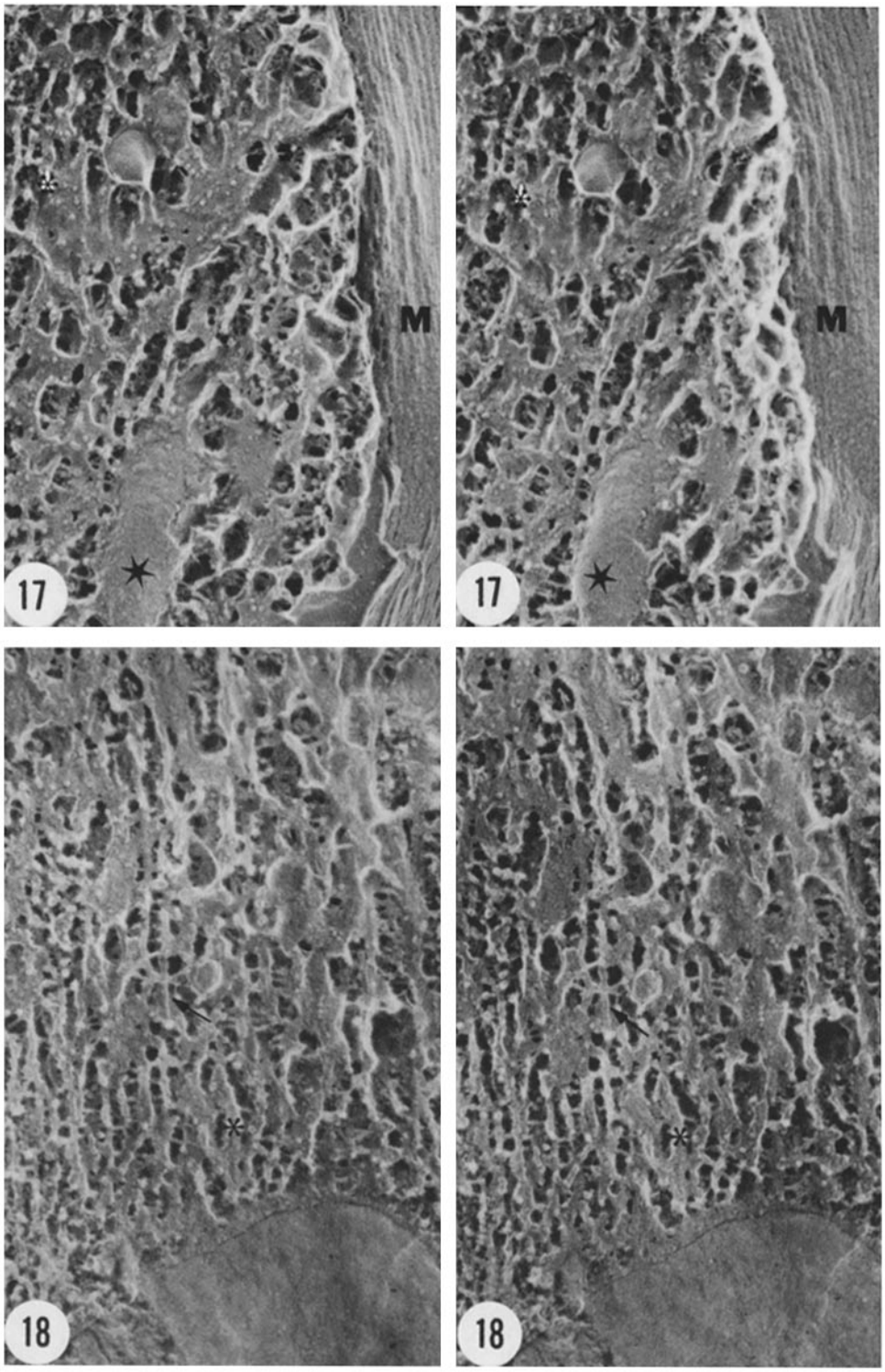


FIGURE 17 Another way of obtaining images of the cross-bridges in the axoplasmic matrix is deep freeze-etching. In such preparations, one can recognize cross-bridging connections emanating from microtubules (asterisk) and neurofilaments. Note the connections to the mitochondrion (star) and the axolemma beneath the myelin sheath (M). × 70,000.

FIGURE 18 A freeze-etch rotary shadow preparation of more longitudinally fractured axoplasm with microtubules (asterisk) and neurofilaments (arrow) interconnected. × 70,000.

## DISCUSSION

Our findings indicate that within axoplasm there is an elaborate system of cross-bridges radiating from microtubules and neurofilaments at approximate right angles. These elements are analogous to the trabecular linkages found in cultured cells but are more highly ordered or periodic. The cross-linking structures appear to be labile at least inasmuch as they are not easy to preserve and stain. For example, our observations that the cross-bridges are more readily visualized after tannic acid

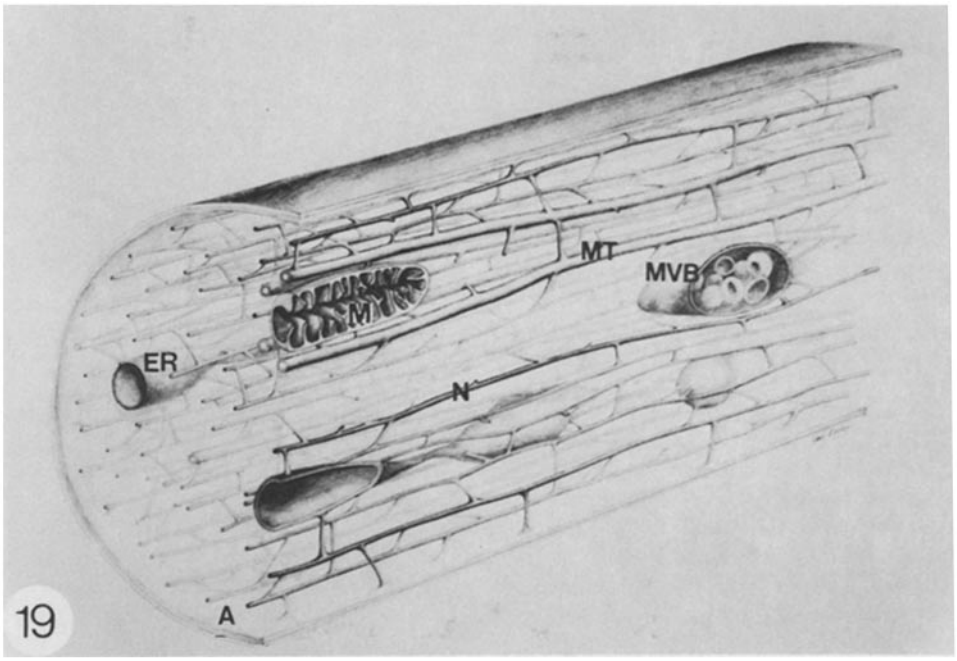


FIGURE 19 A model of the axoplasmic matrix or lattice illustrating the relationship between the cross-bridging elements and other organelles and inclusions. In this model, material of the lattice connects to the axolemma (*A*), the surfaces of elongate and spherical elements of the SER (*ER*), with microtubules (*MT*), neurofilaments (*N*), mitochondria (*M*), and multivesicular bodies (*MVB*). × ~150,000.

mordanting before $OsO_4$ postfixation would be consistent with the observation of Pollard and Maupin (39) that actin will be depolymerized by $OsO_4$ except when prefixed with tannic acid, if these cross-linkages contain actin. A further indication of the labile dynamic nature of this matrix is reflected by the asymmetric distribution of cross-bridges connected to the ends of presumably motile axonal cisternae. Alternatively, this differential distribution may reflect labile or dynamic cisternae. We suggest that both the form of the SER cisternae and the distribution of cross-linkages change during rapid axonal transport. This suggestion is offered with the caution that, although most of our material is fixed by rapid perfusion, the lattice is a labile system and the image we obtain may incorporate its response to environmental changes.

## Axonal Microtrabecular System: Artifact vs. Reality

In a discussion of such fine structures as the MTL of the cytoplasmic ground substance, one must attend to the possibility of artifact. The form of the MTL of cultured cells, preserved by a variety of procedures, has been examined extensively. Detailed observations relating to the artifact-reality controversy may be found in the report by Wolosewick and Porter (58). In this earlier report, the MTL within cultured cells was observed after fixation by aldehyde, $OsO_4$, or rapid-freezing followed by critical point drying or freeze-drying. Although the dimensions of the cross-linking elements varied slightly, the structure was essentially the same, arguing for its reality. When similarly prepared cultured cells were embedded in epoxy resins, the fine cross-linking elements were less apparent, a finding in concordance with the observations of this report. Furthermore, examination of model systems, such as bovine serum albumin or whole erythrocytes after standard fixation procedures, failed to reveal a latticelike condensation of an otherwise homogeneous protein. By extracting consistent morphological features from tissue specimens prepared by different techniques, we have extended earlier studies (58) on the "artifact or reality" of the trabecular lattice in cultured cells to the trabecular structure of axoplasm, a tissue system that is highly specialized for the rapid translocation of compartmentalized material. Thus, our conception of axonal morphology is expanded, and it is appropriate to correlate this new image with the intersection of recent data on the dynamic properties of the trabecular lattice in model systems and the physiology of axonal transport (see below).

## Dynamic Properties of the MTL in Model Systems

As first described by Byers and Porter (5), isolated erythrophores from *Holocentrus asensionis* disperse and aggregate cytoplasmic pigment granules along radially oriented microtubules accompanied by a transformation in the morphology of the MTL. During pigment aggregation, the MTL as a whole appears to contract toward the cell center, whereas during dispersion, the reformation of the MTL appears to carry the granules outward. In a subsequent analysis, the outward motion and associated restructuring of the MTL was found to require cellular ATP whereas the inward motion and associated deformation did not (33). Furthermore, the pigment aggregation and MTL deformation is promoted by increasing $Ca^{++}$ ion concentration, whereas pigment dispersion and MTL reformation are promoted by $Ca^{++}$-depleting buffering systems (34). Preliminary experiments (15) indicate that the axonal microtrabeculae are sensitive to the levels of calcium, magnesium, and ATP in the cytoplasm. These findings are in concordance with observations on the model erythrophore system (34) and cell lines in which the MTL has been studied.

## Rapid Axonal Transport and the Axoplasmic Matrix

A major conceptual breakthrough in neurofilament biochemistry occurred when Hoffman and Lasek (25) suggested that three polypeptides traveling together in the slow component (slow flow, [SCa]) composed a morphological unit, the neurofilament. Thus, these investigators defined proteins that relate to one another in a functional-structural manner. Thus, SCa moving at 1 mm/d primarily contains tubulin and neurofilament proteins, whereas the rapid component, moving at 100–400 mm/d, contains SER cisternae, $Ca^{++}$, synthesized protein, and glycoprotein for transmitter metabolism, export, etc. With the same experimental paradigm, Black and Lasek (2) have described another cluster of polypeptides moving slowly together as a unit but not at the slowest rate; these are the so-called slow component b proteins (SCb). This grouping of macromolecules includes (at this time): actin, clathrin, calmodulin, myosinlike molecules, tropomyosin, brain enolase, and other enzymes of intermediary metabolism. We speculate that these SCb components are likely candidates for some of the major constituents of the axonal matrix or microtrabecular system, largely because this lattice is the only morphological entity occupying a significant enough fraction of the volume of axoplasm not already accounted for by either SCa or the rapid component. Some evidence for certain of these SCb components' being visualizable in the electron microscope by conventional means is available. For example, clathrin is the coat of coated vesicles (37). Calmodulin is periodically distributed in axoplasm (32) along with $Ca^{++}$ densities (14). Immunocytochemical localization of actin to trabeculalike linkages in culture cells has been reported (54). Thus, there is some evidence indicating that SCb components may correlate with the MTL of axoplasm. Ca is transported rapidly and bidirectionally within axoplasm (21) and, in at least one system, concentrations can be localized to cisternae of the axonal SER (22). A Ca requirement for transport has been demonstrated (36) and at least one axoplasmic $Ca^{++}/Mg^{++}$-ATPase has been isolated (28). The specific localization of the SCb components, $Ca^{++}$, and $Ca^{++}$- or $Mg^{++}$-ATPase within this matrix will aid in understanding how these components may interact to provide for the transduction of chemical to kinetic energy for the translocation of materials moved in rapid axonal transport.

## Speculation on a Mechanism for Rapid Axonal Transport

It has been postulated that purified actin gels possessing a morphology similar to that of the trabecular lattice can generate mechanical work according to the "solation-contraction-coupling hypothesis" (7). This hypothetical mechanism may be relevant to axoplasmic transport but would require actin sliding past myosin during cisternal translocation, resulting in a net movement of one contractile element relative to the other. If actin, for example, were attached to SER cisternae and if myosin were relatively stationary, one would expect to find actin in the rapidly transported component and not myosin, or vice versa. This does not appear to be the case, inasmuch as both are found almost exclusively in the same component, SCb (1, 2).

We suggest an alternative mechanism for rapid transport involving controlled local variations in the connectivity of trabecular cross-linkages. The control for such local effects may be the release of $Ca^{++}$ from one end on a motile fragment of SER and $Ca^{++}$ sequestration at the other. Thus, a transport compartment might interact with the axoplasmic matrix differentially on its leading vs. trailing ends. This model would predict a differential distribution of specific regulatory membrane-associated proteins on leading and trailing ends of axonal cisternae, with the information signaling the axonal matrix to act on the membranous element associated with the surface of the cisternae. Some of the metabolic energy for such movements might be spent in the making of cross-bridges and sequestration of $Ca^{++}$ in cisternae.

Any model for rapid transport must accommodate the long saltatory movements of transported material visible in the light microscope and the rapid, selective, and bidirectional nature of transport. Assigning the signal to initiate movement to the cisternae may also help explain the mechanism of bidirectional rapid transport, if different types of compartments for orthograde and retrograde transport are used by the axon. Evidence that morphologically different types of compartments are associated with orthograde and retrograde rapid transport has been presented (46, 51). Furthermore, uniform polarity of microtubules has been demonstrated in at least one axonal system containing only microtubules (6). It is attractive, then, to propose that the different types of compartments (coded for the direction they are to move) recognize axonal cytoskeleton polarity in either microtubules or neurofilaments and their associated trabecular cross-linkages stimulating the trabecular matrix to act upon them, resulting in cisternal translocation in the appropriate direction. With refinements in the techniques of molecular anatomy, one can expect rapid progress in determining the actual mechanisms of rapid neuroplasmic transport.

The authors would like to express appreciation to T. Deerinck, K. Anderson, and G. Wray for assistance in these studies and to J. Logan for the illustration. We would also like to thank D. D. Taitano for her assistance in typing this manuscript.

This work was supported by research grants to Mark H. Ellisman from the National Institutes of Neurological and Communicative Diseases and Stroke (NS-14718) and the Muscular Dystrophy Association of America. The HVEM work was in part supported by a grant from the Biotechnology Research Resources Division of National Institutes of Health to Keith R. Porter (5P41RR00592).

*Received for publication 11 March 1980, and in revised form 9 July 1980.*

## REFERENCES

1. Black, M. M., and R. J. Lasek. 1979. Axonal transport of actin: slow component b is the principal source of actin for the axon. *Brain Res.* 171:401–413.
2. Black, M. M., and R. J. Lasek. 1980. Slow components of axonal transport: two cytoskeletal networks. *J. Cell Biol.* 86:616–623.
3. Broadwell, R. D., C. Oliver, and M. W. Brightman. 1980. Neuronal transport of acid hydrolases and peroxidase within the lysosomal system of organelles: the involvement of agranular reticulum-like cisterns. *J. Comp. Neurol.* 190:519–532.
4. Burton, P. R., and H. L. Fernandez. 1973. Delineation by lanthanum staining of filamentous elements associated with the surfaces of axonal microtubules. *J. Cell Sci.* 12:567–583.
5. Byers, H. R., and K. R. Porter. 1977. Transformations in the structure of the cytoplasmic ground substance in erythrophores during pigment aggregation and dispersion. I. A study using whole-cell preparations in stereo high voltage electron microscopy. *J Cell Biol.* 75: 541–558.
6. Chalfie, M., and J. N. Thomson. 1979. Organization of neuronal microtubules in the nematode *Caenorhabditis elegans*. *J. Cell Biol.* 82:278–289.
7. Condeelis, J. 1980. Reciprocal interactions between the actin lattice and cell membrane. *In* The Cytoskeleton and the Architecture of Nervous Systems, Neurosciences Research Program Workshop. October 22, 1979, The MIT Press, Cambridge, Mass. In press.
8. Cooper, P. D., and R. S. Smith. 1974. The movement of optically detectable organelles in myelinated axons of *Xenopus laeves*. *J. Physiol. (Lond.)*. 242:77-97.
9. Droz, B. 1967. Synthèse et transfert des protéines cellulaires dans les neurons ganglionnaires: étude radioautographique quantitative en microscopie électronique. *J. Microsc. (Paris)*. 6:201–208.
10. Droz, B., A. Rambourg, and H. W. Koenig. 1975. The smooth endoplasmic reticulum: structure and role in the renewal of axonal membrane and synaptic vesicles by fast axonal transport. *Brain Res.* 93:1–13.
11. Ellisman, M. H. 1977. High voltage electron microscopy of cortical specializations associated with the membranes at nodes of Ranvier. *J. Cell Biol.* 75(2, Pt. 2):108 *a* (Abstr.).

12. Ellisman, M. H. 1981. Beyond neurofilaments and microtubules. *In* The Cytoskeleton and the Architectures of Nervous Systems, Neuroscience Research Program Workshop. October 22, 1979, The MIT Press, Cambridge, Mass. 19.
13. Ellisman, M. H., M. H. Brooke, K. K. Kaiser, and J. E. Rash. 1978. Appearance in slow muscle sarcolemma of specializations characteristic of fast muscle after reinnervation by a fast muscle nerve. *Exp. Neurol.* 58:59–67.
14. Ellisman, M. H., P. Friedman, and W. Hamilton. 1980. The localization of sodium and calcium to Schwann cell paranodal loops at nodes of Ranvier and of calcium to compact myelin. *J. Neurocytol.* 9:185–205.
15. Ellisman, M.H., and K. R. Porter. 1979. New techniques for revealing the cytoskeleton of axoplasm and the effects of $Ca^{++}$ upon its organization. *Neuroscience Abstracts.* 5:59.
16. Ellisman, M. H., and L. A. Staehelin. 1979. An electronically interlocked electron gun shutter for preparing improved replicas of freeze-fracture specimens. *In* Preparation Dependent Chances in Freeze-Fracture. J. E. Rash, and C. S. Hudson, editors. Raven Press, New York. 123–126.
17. Forman, D. S., A. L. Padjen, and G. R. Siggins. 1977. Axonal transport of organelles visualized by light microscopy: cinemicrographic and computer analysis. *Brain Res.* 136: 197–213.
18. Forman, D. S., A. L. Padjen, and G. R. Siggins. 1977. Effect of temperature on the retrograde transport of microscopically visible intraaxonal organelles. *Brain Res.* 136:215–226.
19. Friedman, P. L., and M. H. Ellisman. 1980. Enhanced visualization of peripheral nerve, neuropil and sensory receptors in the scanning electron microscope using cryofracture and osmium-thiocarbohydrazide-osium impregnation. *J. Neurocytol.* In press.
20. Grafstein, B., and D. S. Forman. 1980. Intracellular transport in neruons. *Physiol. Rev.* In press.
21. Hammerschlag, R., A. Y. Chiu, B. Weiss, and A. R. Dravid. 1976. Axonal translocation of $^{45}Ca^{++}$: relation to fast transport of protein. *Neuroscience Abstracts.* 2:36.
22. Henkart, M., T. S. Reese, and F. J. Briney. 1978. Endoplasmic reticulum sequesters $Ca^{++}$ in squid giant axon. *Science (Wash. D. C.).* 202:1300–1303.
23. Heslop, J. P. 1975. Axonal flow and fast transport in nerves. *Adv. Comp. Physiol. Biochem.* 6:75–163.
24. Heuser, J. E., and S. R. Salpeter. 1979. Organization of acetylcholine receptors in quick-frozen, deep-etched, and rotary-replicated *Torpedo* postsynaptic membrane. *J. Cell Biol.* 82:150–173.
25. Hoffman, P. N., and R. J. Lasek. 1975. The slow component of axonal transport. Identification of major structural polypeptides of the axon and their generality among mammalian neurons. *J. Cell Biol.* 66:351–356.
26. Holtzman, E. 1977. The orgin and fate of secretory packages especially synaptic vesicles. *Neuroscience.* 2:327–355.
27. Karlsson, J. O., and J. Sjostrand. 1971. Transport of microtubular protein in axons of retinal ganglion cells. *J. Neurochem.* 18:975–982.
28. Khan, M. A., and S. Ochs. 1974. Magnesium or calcium activated ATPase in mammalian nerve. *Brain Res.* 81:413–426.
29. Lane, N. J., and J. E. Treherne. 1970. Lanthanum staining of neurotubules in axons from cockroach ganglia. *J. Cell Sci.* 7:217–231.
30. Lasek, R. J., and P. N. Hoffman. 1976. The neuronal cytoskeleton, axonal transport and axonal growth. *Cold Spring Harbor Conf. Cell Proliferation.* 3(Book A):1021–1049.
31. Levin, B. E. 1978. Axonal transport of [$^3$H]proteins in a noradrenergic system of the rat brain. *Brain Res.* 150:55–68.
32. Lin, C. T., J. R. Dedman, B. R. Brinkley, and A. R. Means. 1980. Localization of calmodulin in rat cerebellum by immunoelectron microscopy. *J. Cell. Biol.* 85: 473–480.
33. Luby, K. J., and K. R. Porter. 1980. The control of pigment migration in isolated erythropores of *Holocentrus ascensionis* (Osbeck). I. Energy requirements. *Cell.* In press.
34. Luby, K.J. 1980. The role of $Ca^{++}$ in the control of pigment migration in *Holocentrus* erythrophores. Second International Congress on Cell Biology, Berlin. In press.
35. Metuzals, J. 1969. Configuration of a filamentous network in the axoplasm of the squid (*Loligo paelii L.*) giant nerve fiber. *J. Cell Biol.* 43:480–505.
36. Ochs, S., R. M. Worth, and S. Y. Chan. 1977. Calcium requirement for axoplasmic transport in mammalian nerve. *Nature (Lond.).* 270:748–750.
37. Pearse, B. M. F. 1975. Coated vesicles from pig brain: purification and biochemical characterization. *J. Mol. Biol.* 97:93–98.
38. Peters, A. 1966. The node of Ranvier in the central nervous system. *Q. J. Exp. Physiol. Cogn. Med. Sci.* 51:229–236.
39. Pollard, T. C., and P. Maupin. 1978. Electron microscopy of cytoplasmic contractile proteins. Ninth International Congress on Electron Microscopy, Toronto, 1978. 3:606–614.
40. Pomerat, C. M., W. J. Hendelman, C. W. Rainborn, Jr., and J. F. Massey. 1967. Dynamic activities of nervous tissue *in vitro*. *In* The Neuron. H. Hyden, editor. Elsevier/North Holland Biomedical Press, Amsterdam. 119–178.
41. Porter, K. R. 1976. Introduction: motility in cells. *Cold Spring Harbor Conf. Cell Proliferation.* 3(Book A):1–28.
42. Porter, K. R., H. R. Byers, and M. H. Ellisman. 1979. The cytoskeleton. *In* The Neurosciences, Fourth Study Program. F. O. Schmitt, and F. G. Worden, editors. The MIT Press, Cambridge, Mass. 703–722.
43. Sannes, P. L., J. Katsuyama, and S. S. Spicer. 1978. Tannic acid-metal salt sequences for light and electron microscopic localization of complex carbohydrates. *J. Histochem. Cytochem.* 26:55–61.
44. Simionescu, N., and M. Simionescu. 1976. Galloylglucoses of low molecular weight as mordant in electron microscopy I. Procedure, and evidence for mordanting effect. *J. Cell Biol.* 70:608–621.
45. Smith, D. S. 1971. On the significance of crossbridges between microtubules and synaptic vesicles. *Philos. Trans. R. Soc. Lond. B Biol. Sci.* 261:395–405.
46. Smith, R. S. 1980. The short term accumulation of axonally transported organelles in the region of localized lesions of single myelinated axons. *J. Neurocytol.* 9:39–65.
47. Smith, R. S., U. Jarlfors, and R. Beranek. 1970. The organization of synaptic axoplasm in lamprey (*Petromyzon marinus*) central nervous system. *J. Cell Biol.* 46:199–219.
48. Tani, E., and T. Ametani. 1970. Substructure of microtubules in brain nerve cells as revealed by ruthenium red. *J. Cell Biol.* 46:159–165.
49. Thoenen, H., U. Otten, and M. Schwab. 1979. Orthograde and retrograde signals for the regulation of neuronal gene expression: the peripheral sympathetic nervous system as a model. *In* The Neurosciences Fourth Study Program. F. O. Schmitt, and F. G. Worden, editors. The MIT Press, Cambridge, Mass.
50. Tsukita, S., and H. Ishikawa. 1976. Three-dimensional distribution of smooth endoplasmic reticulum in myelinated axons. *J. Electron Microsc.* 25:141–419.
51. Tsukita, S., and H. Ishikawa. 1980. The movement of membranous organelles in axons. Electron microscopic identification of anterogradely and retrogradely transported organelles. *J. Cell Biol.* 84:513–530.
52. Van Harreveld, A., and J. Crowell. 1964. Electron microscopy after rapid freezing on a metal surface and substitution fixation. *Anat. Rec.* 149:381–386.
53. Van Harreveld, A., J. Trubatch, and J. Steiner. 1974. Rapid freezing and electron microscopy for the arrest of physiological processes. *J. Microsc. (Oxf).* 100:189–198.
54. Webster, R. E., P. Henderson, M. Osborn, and K. Weber. 1978. Three-dimensional electron microscopical visualization of the cytoskeleton of animal cells: immunoferritin identification of actin and tubulin containing structures. *Proc. Natl. Acad. Sci. U. S. A.* 75: 5511–5515.
55. Willard, M., W. M. Cowan, and P. R. Vagelos. 1974. The polypeptide composition of intraaxonally transported proteins: evidence for four transport velocities. *Proc. Natl. Acad. Sci. U. S. A.* 71:2183–2187.
56. Willard, M. B., and K. L. Hulebak. 1977. The intra-axonal transport of polypeptide H: evidence for a fifth (very slow) group of transported polypeptides in the retinal ganglion cells of the rabbit. *Brain Res.* 136:289–306.
57. Wolosewick, J. J. 1980. The application of polyethylene glycol (PEG) to electron microscopy. *J. Cell Biol.* 86:675–681.
58. Wolosewick, J. J., and K. R. Porter. 1979. Microtrabecular lattice of the cytoplasmic ground substance. Artifact or reality. *J. Cell Biol.* 82:114–139.
59. Wuerker, R. B., and S. L. Palay. 1969. Neurofilaments and microtubules in anterior horn cells of the rat. *Tissue Cell.* 11:387–402.
60. Yamada, K. M., B. S. Spooner, and N. K. Wessells. 1971. Ultrastructure and function of growth cones and axons of cultured nerve cells. *J. Cell Biol.* 49:614–635.